Materials and Design 37 (2012) 402–409

Contents lists available at SciVerse ScienceDirect

Materials and Design

journal homepage: www.elsevier.com/locate/matdes

Analysis of high temperature plastic behaviour and its relation with weldability in friction stir welding for aluminium alloys AA5083-H111 and AA6082-T6

C. Leitão [a], R. Louro [b], D.M. Rodrigues [a,*]

[a] CEMUC, Mechanical Engineering Department, University of Coimbra, Portugal
[b] ISQ, Welding and Quality Institute, Portugal

ARTICLE INFO

Article history:
Received 13 December 2011
Accepted 16 January 2012
Available online 24 January 2012

Keywords:
Welding
Plastic behaviour
Thermal analysis

ABSTRACT

The influence of the plastic behaviour of two aluminium alloys, very popular in welding construction, on friction stir weldability, is analysed in this work. The two base materials, a non-heat-treatable (AA5083-H111) and a heat-treatable aluminium (AA6082-T6) alloy, are characterised by markedly different strengthening mechanisms and microstructural evolution at increasing temperatures. Their plastic behaviour, under different testing conditions, was analysed and compared. The two base materials were also welded under varied friction stir welding (FSW) conditions in order to characterise their weldability. The relation between weldability, material flow during FSW and the plastic behaviour of the base materials, at different temperatures, was analysed. It was found that the AA6082 alloy, which displays intense flow softening during tensile loading at high temperatures, and is sensitive to dynamic precipitation and overageing under intense non-uniform deformation, displays good weldability in FSW. Under the same welding conditions, the AA5083 alloy, which in quasi-static conditions displays steady flow behaviour at increasing temperatures, and is sensitive to moderate hardening at high strain rates, displays poor weldability.

1. Introduction

The establishment of accurate relationships between base materials plastic behaviour, process parameters and weld characteristics is still an almost unexplored topic in friction stir welding (FSW) research. Actually, despite being a solid state process, in which plastic deformation plays a major role in the joining mechanisms, studies relating the plastic behaviour of the base materials with material flow and/or heat generation during the process are still very scarce. In fact, over the past decade, most of published literature on FSW was focused on the microstructural and mechanical characterisation of the welds, on the understanding of the material flow mechanisms and on the analysis of the heat generation and dissipation during the process [1]. Concerning this last aspect, regardless of being currently accepted that heat generation during the process results simultaneously from friction and plastic deformation, there is still no consensus regarding which will be the dominant heat generation mechanism or the prevalent contact condition at the tool/workpiece interface [2–7].

Actually, establishing relations between plastic behaviour and material flow during FSW is a very difficult task, either by experimental means or by numerical simulation, due to the high difficulty in characterising the plastic behaviour of the materials at the temperatures and strain rates attained during FSW. Despite these huge difficulties, significant efforts in understanding the thermal histories and temperature distributions in the welds were already spent, using both experimental work and numerical predictions [2–5,7–15]. A common feature to almost all the numerical works was the difficulty in previewing the maximum temperature attained in the process. This problem is usually overcome by using different modelling alternatives, such as adapting the heat generation models, heat exchange coefficients and/or the tool-workpiece contact conditions. However, any possible influence of the plastic properties of the materials in heat-generation and/or friction stir weldability is not fully explored and/or understood.

Balasubramanian et al. [16,17] were the first in developing empirical relationships between base materials properties and friction stir weldability. However, their relations only take into account base material properties such as hardness, yield strength, tensile strength and maximum elongation, all at room temperature, which are not sufficient for fully characterising base material plastic behaviour in FSW conditions.

In a previous work from current authors [18], important differences in friction stir weldability between two aluminium alloys often used in welding construction, the non-heat-treatable AA5083-H111 and the heat-treatable AA6082-T6 aluminium alloys, were depicted. Since both alloys were welded under similar

* Corresponding author. Tel.: +351 239 790 700; fax: +351 239 790 701.
E-mail address: dulce.rodrigues@dem.uc.pt (D.M. Rodrigues).

0261-3069/$ - see front matter © 2012 Elsevier Ltd. All rights reserved.
doi:10.1016/j.matdes.2012.01.031

processing conditions, the differences in base materials plastic properties were pointed as the main factor in determining the different welding behaviour. So, in a subsequent work, which is described in current paper, the plastic behaviour of the two base materials was deeply analysed by performing mechanical characterisation tests under varied temperatures and loading conditions. Thermal simulation tests were also conducted, for both base materials, replicating heating conditions close to that occurring during FSW. Finally, the morphology of welds obtained for the two base materials was deeply analysed and compared. Based on base materials mechanical characterisation results, weld characteristics and on authors past experience on FSW material flow analysis [19,20] and microstructural and mechanical characterisation of 5xxx and 6xxx friction stir welds [21–24], important relations between base materials plastic properties and weld characteristics were established, which will be described in the next. First, the friction stir welding results, for both alloys, are compared, and after that, the main differences in weldability are enhanced and explained based on base materials plastic properties at high temperature.

2. Experimental procedure

2.1. Welding tests

In order to analyse the weldability of the AA5083-H111 and AA6082-T6 base materials, supplied in 6 mm thick plates, they were welded using different tools and process parameters. Since the material flow mechanisms in FSW with conical tools are already well known [19], which is important for establishing relations between it and the plastic behaviour of the base materials during welding, conical shoulder tools, with cone angle of 5° and cylindrical threaded pins, were used. The welding speed (v), rotating speed (w), vertical force (F_z), shoulder and pin diameters (D_s and D_p, respectively) and tool pitch angle (α) were varied according to Table 1. Bead-on-plate welds were produced in order to eliminate the influence of sheet positioning and clamping on welding test results.

The testing plan (Table 2), established by combining the different tool and processing parameters, determined a total of 36 welds to be performed for each base material. After welding, all welds were visually inspected for identifying surface defects like flash and surface flaws. Transverse specimens were also cut from the welds, cold mounted, polished, etteched and observed using the Zeiss Stemi 2000-C and Zeiss Axiotech 100HD microscopes, for detecting large and very small internal flaws as well as for analysing welds morphology.

2.2. Mechanical characterisation test

The plastic behaviour of the AA5083 and AA6082 alloys was analysed by performing tensile and shear tests. The tensile tests were performed using Instron 8800 FastTrack and Instron 4206 machines, in accordance with the ASTM E8 M and ASTM E21 standards [25,26]. The testing speed was 5 mm/min and the testing temperatures ranged from room temperature to 500 °C. The temperature was controlled using a thermocouple placed inside the convection oven, directly in contact with the surface of the samples. The shear tests were performed under quasi-static conditions, with 5 mm/min testing speed, in an Instron 4206 machine, by using a tool specially developed for testing thick material samples. Strain data acquisition was performed using ARAMIS Optical 3D Deformation & Strain Measurement system. Finally, micro-hardness measurements, in selected areas of the mechanical testing samples and of the welds, were performed using a Shimadzu – Micro-Hardness Tester with 200 gf load for 30 s.

Table 1
Friction stir welding parameters.

Tool parameters	Pin diameter (D_p) (mm)			Shoulder diameter (D_s) (mm)			Tilt angle (α (°))		
	6	7		15	18	21	1	2	3
Process parameters	Weld speed (v), mm min^{-1}			Rotational speed (w) (rpm)			Axial force (F_z) (kN)		
	200	275	350	300	400	500	10	15	20

Table 2
Welding plan.

	D_p (mm)	D_s (mm)	α (°)	v (mm min^{-1})	w (rpm)	F_z (kN)
1	6	15	1	200	300	10
2	6	15	2	200	400	15
3	7	15	3	200	500	20
4	7	18	1	200	300	10
5	6	18	2	200	400	15
6	6	18	3	200	500	20
7	7	18	1	200	300	15
8	7	18	2	200	400	20
9	6	18	3	200	500	10
10	6	21	1	200	300	20
11	7	21	2	200	400	10
12	7	21	3	200	500	15
13	6	15	1	275	400	20
14	6	15	2	275	500	10
15	7	15	3	275	300	15
16	7	18	1	275	400	20
17	6	18	2	275	500	10
18	6	18	3	275	300	15
19	7	18	1	275	400	10
20	7	18	2	275	500	15
21	6	18	3	275	300	20
22	6	21	1	275	400	15
23	7	21	2	275	500	20
24	7	21	3	275	300	10
25	6	15	1	350	500	15
26	6	15	2	350	300	20
27	7	15	3	350	400	10
28	7	18	1	350	500	15
29	6	18	2	350	300	20
30	6	18	3	350	400	10
31	7	18	1	350	500	20
32	7	18	2	350	300	10
33	6	18	3	350	400	15
34	6	21	1	350	500	10
35	7	21	2	350	300	15
36	7	21	3	350	400	20

3. Results and discussion

3.1. Friction stir welding results

Visual inspection and metallographic analysis enabled to identify non-defective welds (examples in Fig. 1a–c and e) and three main types of defects: internal flaws and flash (examples in Fig. 1d, g and h), for both base materials, and surface flaws (example in Fig. 1f), for the AA5083 welds. The full range of welding inspection results are summarised in the graphs of Fig. 2 and 3, where the pressure (P) versus rotation to traverse speed ratio (w/v), for all welding test conditions, are plotted. The pressure parameter, which was calculated using the equation:

$$P = \frac{F_z}{\frac{\pi}{4}(D_s^2 - D_p^2)} \quad (1)$$

reflects the influence of the axial load (F_z) and tool parameters (D_s and D_p) on welding results. In the graph, the acceptable welds,

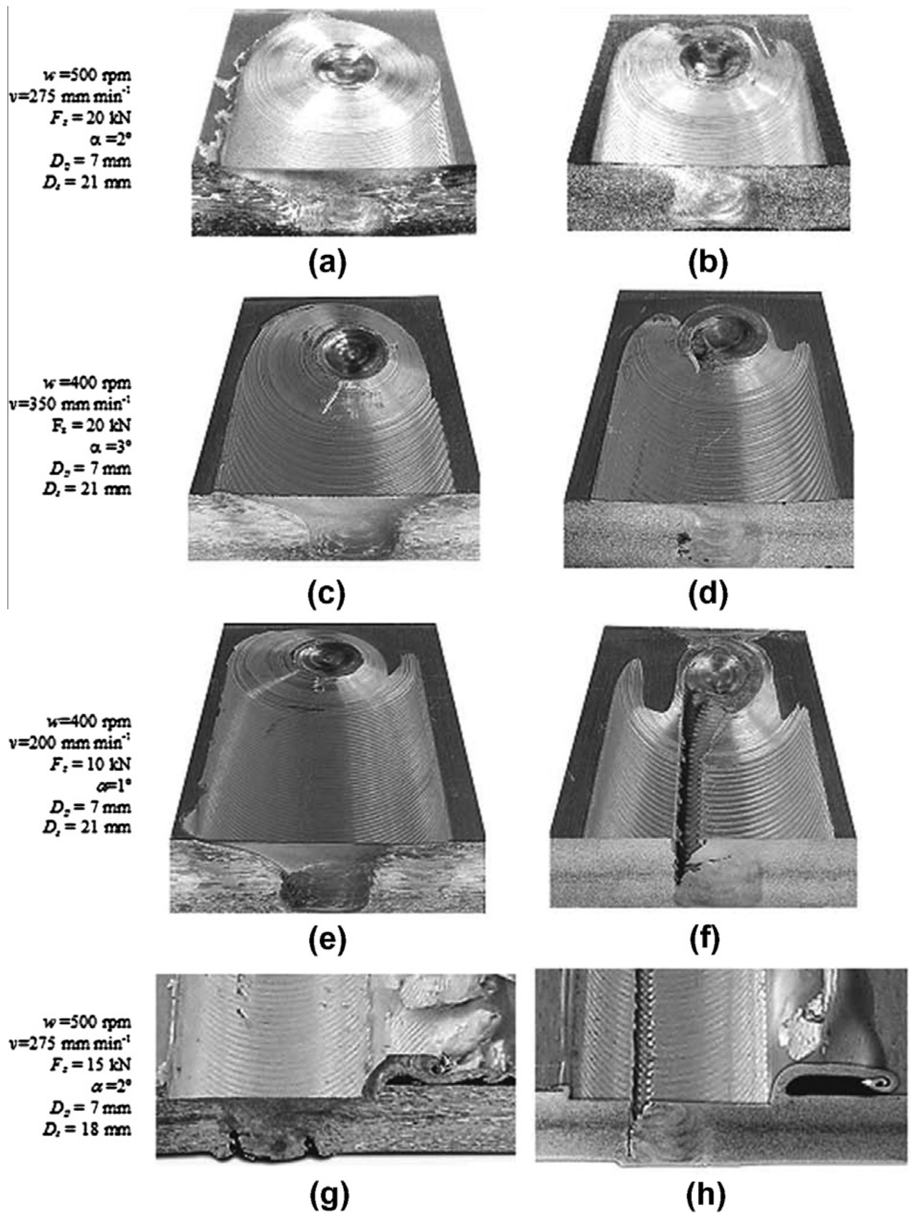

Fig. 1. Top views and cross-sections of AA 6082 (a, c, e and g) and AA 5083 (b, d, f and h) welds.

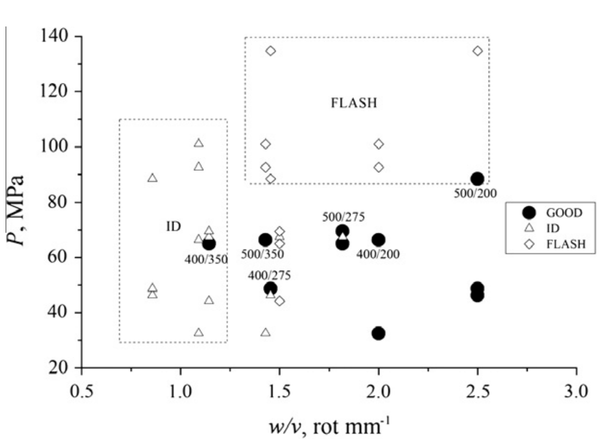

Fig. 2. Welding results for the AA6082 alloy.

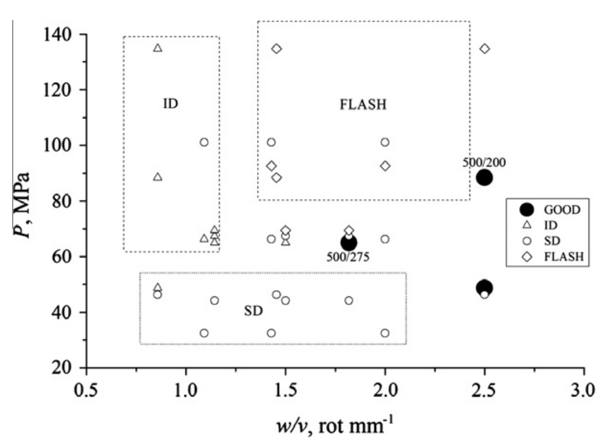

Fig. 3. Welding results for the AA5083 alloy.

named GOOD welds, are identified using large black symbols, and the welds with defects, by using smaller symbols of different types. The results identified as GOOD also comprise welds with very small defects, which were not considered important for the global strength of the welded plates [18]. The tool rotation to traverse speed (w/v) ratio, corresponding to the GOOD welding results, are also explicitly identified in the graph. Comparing Figs. 2 and 3, relative to the AA6082 and AA5083 alloy, respectively, it is possible to conclude that, for the range of welding parameters tested in this work, the AA6082 base material have higher weldability than the AA5083 base material, since a larger number of GOOD welds was obtained for that alloy. Actually, it is possible to observe that meanwhile for the AA5083 alloy, it was impossible to obtain GOOD welds using the tool rotation rates of 300 and 400 rpm and the tool traverse speed of 350 mm/min, for the AA6082 alloy, it was only impossible to obtain GOOD welds using the tool rotation speed of 300 rpm. However, it is important to remark that the number of non-acceptable welds was very high for both alloys, showing that the process is very sensitive to the combination of tool and machine parameters.

In Figs. 2 and 3, process parameter domains, corresponding to a larger incidence of each defect type, were delimited. Comparing the pictures it is possible to conclude that, for both base materials, flash was mainly formed for the higher values of w/v, corresponding to the higher heat input conditions, and for the higher values of pressure, P, corresponding to the use of the smaller shoulder diameter tool (D_s = 15 mm). For the lower w/v values, internal flaws (ID) were the main type of defect detected for both alloys. However, for the AA5083 alloy, for almost the entire range of w/v values, surface flaws (SD) were also detected for the lower pressure conditions, corresponding to the utilisation of very low axial loads (10 and 15 kN). In contrast, for the AA6082 alloy, no strong limitation in axial load was found, being possible to obtain GOOD welds for all the loads tested. Finally, defects of varying types, according to the global combination of process parameters, were detected for the welds performed with tool tilt angle α = 1°. These situations, which are not explicitly identified in Figs. 3 and 4, justify some dispersion of the weld inspection results in both graphs.

Another important conclusion, which can be drawn from present work, is the existence of a close relation between weld morphology and base material type. Actually, comparing the pictures in Fig. 1, where AA6082 and AA5083 weld cross sections are displayed, it can be depicted a completely different morphology for welds performed under exactly the same welding conditions. As it is possible to observe in the figure, independently of the welding conditions, the weld cross-sections are wider for the AA6082 plates, being characterised by a well-defined shoulder influence zone, extending to the mid-plates thickness. Instead, for the AA5083 welds, the TMAZ is almost restricted to the pin influence zone with a very small evidence of material being dragged by the shoulder. In previous works [4,5,10,27,28], the evolution of welds morphology and dimensions was related with the variation in welding parameters. However, since each pair of welds shown in Fig. 1 was performed using exactly the same welding conditions, it is from now possible to say that the weld morphology also depends on base material properties.

In Fig. 1 it is also shown, for each weld, the final print left by the tool at the end of the welding operation. As it is possible to conclude from the figure, for the AA6082 weld, the shoulder mark is almost perfectly round, except for the lower axial load weld (Fig. 1.e), showing that the material was dragged easily by the shoulder. For the AA5083 weld, the final print left by the shoulder clearly shows that the shoulder-workpiece contact area was restricted to the trailing side of the tool, especially for the cold welds, performed at 400 rpm (Fig. 1d and f). Again, since the AA6082 and AA5083 welds were performed under the same welding conditions, the differences in contact conditions have to be related with intrinsic base material properties.

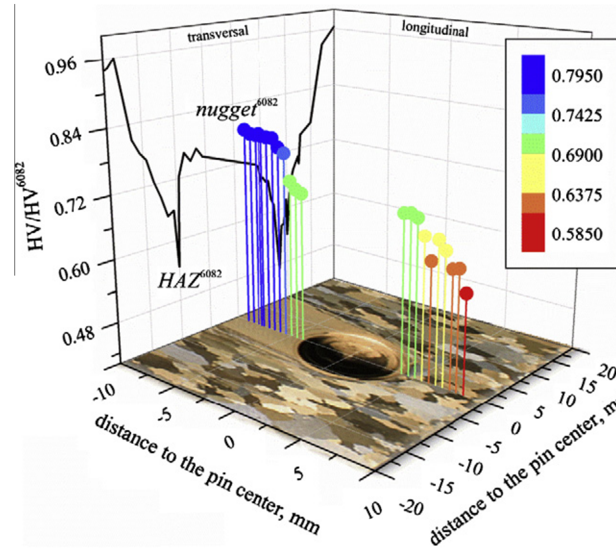

Fig. 4. Transverse and longitudinal hardness for a AA6082 weld. Welding conditions: w = 500 rpm, v = 275 mm min^{-1}, F_z = 20 kN, α = 2°, D_p = 7 mm and D_s = 21 mm. HV^{6082} is the initial base material hardness.

In Figs. 4 and 5 are shown transverse and longitudinal hardness profiles, obtained near the end of the weld, where is located the final hole left by the pin, for the welds in Fig. 1a and b. Actually, these welds will be used as reference in the comparative analysis to be developed in the next items, since they were performed using welding parameters which enabled to obtain non-defective welds for both base materials. Fig. 4 shows that the AA6082 weld display the W shape hardness profile characteristic of the heat-treatable alloys friction stir welds, which was already deeply analysed by Sato et al. [29] and Upadhyay and Reynolds [30] in previous publications. From the figure it is possible to confirm that the intense hardness drop in the HAZ, relative to the initial base material hardness (HV^{6082}), extends to the front of the tool where the tool dragging action will be exerted. For the AA5083 welds, no variation

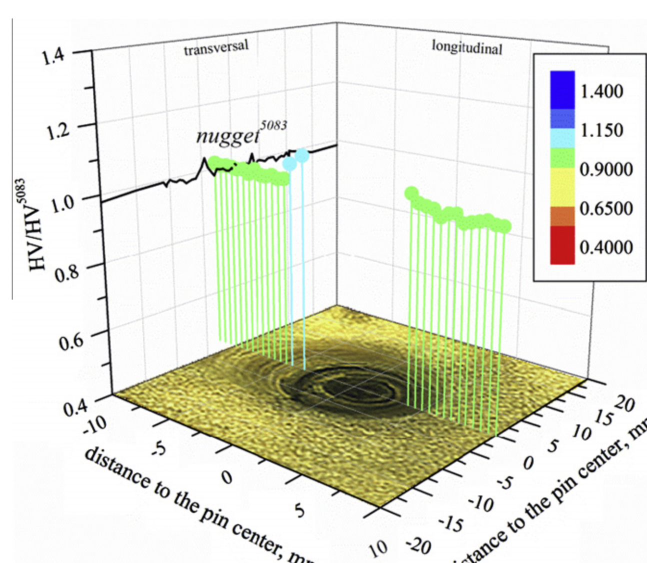

Fig. 5. Transverse and longitudinal hardness for a AA5083 weld. Welding conditions: w = 500 rpm, v = 275 mm min^{-1}, F_z = 20 kN, α = 2°, D_p = 7 mm and D_s = 21 mm. HV^{5083} is the initial base material hardness.

relative to the initial base material hardness (HV^{5083}) was registered, nor in the TMAZ, nor in the HAZ surrounding the tool, as can be depicted from Fig. 5. The hardness evolution for AA5xxx friction stir welds was already deeply analysed in literature [23].

3.2. Mechanical characterisation results

In Fig. 6 are shown stress–strain curves for both base materials, obtained in tension and shear, at room temperature in quasi-static conditions (5 mm min^{-1}). Analysing the curves it is possible to conclude that the AA5083 alloy displays much lower yield strength than the AA6082 alloy, in both shear and tension. However, despite displaying much lower tensile yield strength, the AA5083 alloy exhibits strong Portevin-Le Châtelier effect and pronounced hardening with plastic deformation, attaining tensile strength values very close to that of the AA6082 alloy. From the shear test results, which enable to compare the plastic behaviour of both base materials until values of plastic deformation higher than that attained in tension, it can be concluded that, meanwhile for the AA6082 alloy, an almost steady-state flow stress is attained after moderate values of plastic deformation, for the AA5083 alloy, the flow stress keeps increasing with loading, attaining values higher than that registered for the AA6082 alloy. Inside the graph of Fig. 6 is also show a smaller graph where the hardness registered for the tensile and shear samples, of both base materials, before and after plastic deformation, is compared. The hardness values for the deformed samples are that measured near the rupture section, where extreme values of plastic deformation were attained. From the graph it is possible to conclude that despite the hardness values relative to the non-deformed alloys are very different ($HV^{5083} = 87\ Hv_{0.2}$ and $HV^{6082} = 120\ Hv_{0.2}$), they become similar after plastic deformation. In fact, meanwhile for the AA5083 alloy, the hardness strongly increases with plastic deformation, for the AA6082 alloy, the hardness registered for the deformed and non-deformed samples is very similar. These hardness results enhance again the higher sensitivity of the AA5083 alloy to strain hardening.

Since FSW involves plastic deformation at high temperatures, the plastic behaviour of the base materials was also analysed at temperatures ranging from 240 to 500 °C. In Fig. 7 are shown the engineering stress–strain curves corresponding to the tensile tests performed at temperatures ranging from 240 °C to 500 °C, for the AA5083 alloy, and from 240 °C to 400 °C, for the AA6082 alloy. Inserted in the graph is also shown the evolution of the yield stress (Y_0) with temperature, for both base materials. From both graphs it is possible to conclude that, for the tensile testing conditions used, the yield strength of the base materials become closer at increasing temperatures. It is also possible to observe that the AA6082 alloy displays much smaller strain to failure, than the AA5083 alloy, for the entire range of temperatures. Actually, meanwhile the plastic behaviour of the AA6082 alloy is characterised by strong work softening after peak stress values very close to the yield stress, the plastic behaviour of the AA5082 alloy is characterised by strong work hardening with plastic deformation, at 240 °C, and almost steady flow stress behaviour at the higher temperatures (300–500 °C).

It is well known that, for sufficiently high deformation temperatures, dynamic recovery, and in particular conditions, dynamic recrystallisation, take place during plastic deformation [31], promoting the steady flow stress behaviour registered in Fig. 7, for the AA5083 non-heat treatable alloy. For the heat-treatable alloys, in artificially aged condition, like the AA6082-T6 alloy, concomitantly to dynamic recovery and/or dynamic recrystallisation phenomena, dynamic precipitation also takes place during hot plastic deformation [32]. Dynamic precipitation, which is faster than precipitation in static conditions, due to the increased particle diffusion coefficients in the presence of dense dislocation tangles, easily promotes overageing of the artificially aged microstructure resulting in intense softening with plastic deformation [33], as was registered for the AA6082 alloy, in Fig. 7. According to Wouters et al. [34], the very low ductility experienced by the AA6082 alloy in the high temperature tests should also be related with intense coarsening of precipitates. The mechanisms of failure by coalescence of microvoids, due to localised strain discontinuities, such as that associated with second phase particles, grain boundaries, and dislocation pile-ups, are well documented in literature [35].

4. Analysis of plastic behaviour versus weldability

During friction stir welding, once steady state welding conditions are attained, the dragging action of the tool over the base material will develop under constant load [14]. So, it is reasonable to assume that the AA6082 alloy, which experiences strong softening with plastic deformation at increasing temperatures, will have good weldability in FSW since it will easily undergo intense plastic deformation under constant load, for a large range of temperatures. In opposition, the AA5083 alloy, which displays work-hardening until 240 °C and steady flow stress at higher temperatures, will

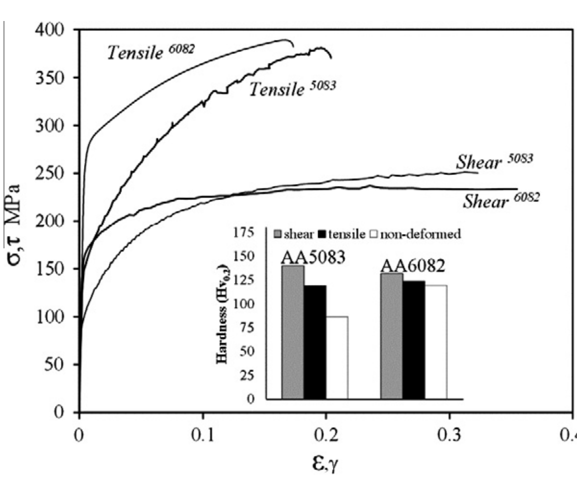

Fig. 6. Base materials tensile and shear stress–strain curves ($T = 25$ °C, 5 mm min^{-1}).

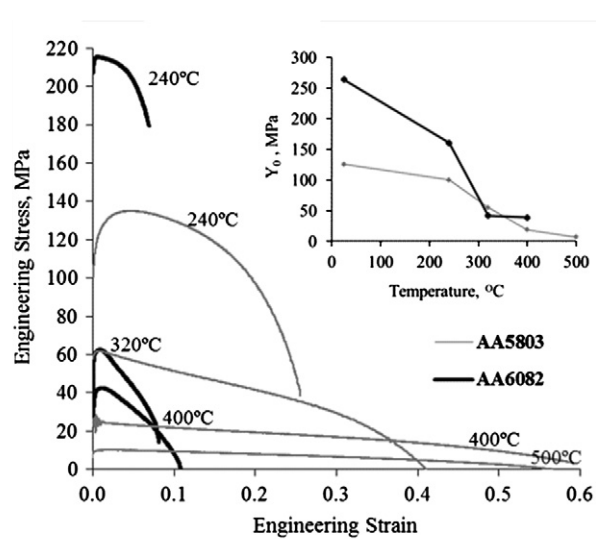

Fig. 7. Engineering tensile stress–strain curves and evolution of base materials yield stress with temperature.

be less efficiently deformed under constant loading conditions. Effectively, comparing the weld shapes displayed in Fig. 1, it is possible to depict that, independently of the welding conditions, the nugget of the welds is much broader for the AA6082 alloy, than for the AA5083 alloy, which corroborates the previous assumptions.

For the AA6082 welds it is even possible to identify in each weld cross-section of Fig. 1 a wide zone of severely deformed but non-recrystallised TMAZ material, which also evidences the intense plastic deformation of this material at temperatures lower than that attained in the nugget. For the AA5083 alloy, nor a deep shoulder influence zone, nor a wide non-recrystallised TMAZ, are visible in any of the welds cross-sections, which also points for the lower efficiency of the tool in dragging the AA5083 base material. Finally, it is also important to consider that the AA6082 alloy displayed very low ductility at high temperatures, which was already related with microvoid coalescence at the grain and large particle boundaries. Assuming that this microvoid coalescence mechanisms are active during FSW, due to intense plastic deformation taking place, the mixing of the materials from the pin and shoulder flow layers should be facilitated by the internal decohesion of the material. Again, material mixing from different flow layers will be much more difficult for the AA5083 alloy, which displays continuous plastic deformation and very high elongation at increasing temperatures.

Despite the important differences in plastic behaviour at high temperatures depicted from the mechanical characterisation work, and the possible relation between it and the material flow behaviour during FSW pointed in previous paragraphs, it is important to observe that the heating and cooling conditions to which the materials were subjected before and after tensile testing are much gentler than that experienced by the materials during FSW. Actually, since the plastic behaviour of the AA6082 alloy is conditioned by solubilisation and precipitation mechanisms, which are strongly time and temperature dependent, an important question is whether at the very fast heating and loading conditions experienced during FSW, the flow softening mechanism discussed during Fig. 7 analysis will be active.

In order to analyse the sensitivity of the AA6082 alloy to overageing at very high heating rates, very small samples of the AA6082 alloy were heated at 30 °Cs^{-1} using a Theta 5528 vertical infra-red furnace. The volume of each sample was approximately 90 mm^3 with a cross-section of 3 × 3 mm and the testing temperatures ranged from 240 °C to 600 °C. The use of very small samples and very fast heating conditions intended to simulate the very small volume of material processed by the FSW tool at each revolution and the fast heating conditions experienced during welding. According to previous studies [2,7,36], the heating rates in the thermal simulation tests were even higher than that experienced during welding. After cooling and some days of natural ageing, the hardness of the thermal simulation samples was evaluated. In Fig. 8 is plotted the evolution of the hardness ratio HV/HV^{6082} with temperature, for all the thermal (*Thermal*^{6082} results) and mechanical (*Tensile*^{6082} and *Shear*^{6082} results) testing samples studied in this work. Analysing the results corresponding to the thermal simulation samples, it is possible to conclude that for temperatures ranging from 240 to 400 °C, which are much lower than the solubilisation temperature of the AA6xxx alloys, which ranges from 510 °C to 595 °C, the hardness registered for the very small thermal simulation samples is already lower than that of the base material (HV/HV^{6082} ≅ 0.90). For the 500 and 600 °C thermal simulation samples, which according to references [2,10,13,36–38] were heated to temperatures in the range of that under the tool during FSW, the hardness is much lower than that of the base material (HV/HV^{6082} ≅ 0.45), which point for the occurrence of overageing at heating rates much higher than that experienced in FSW. In Fig. 8 is also plotted a line (*HAZ*^{6082}) corresponding to the average hardness ratio of the HAZ, in front of the tool, obtained from the hardness profile in Fig. 4. It is possible to see that the average hardness for the 300 and 400 °C tensile samples and for the 500 and 600 °C thermal simulation samples is very close to that of the HAZ. So, it is reasonable to assume that despite being subjected to different thermal cycles, the materials of the different samples are characterised for having the same overaged structure, and in this way, the same plastic properties.

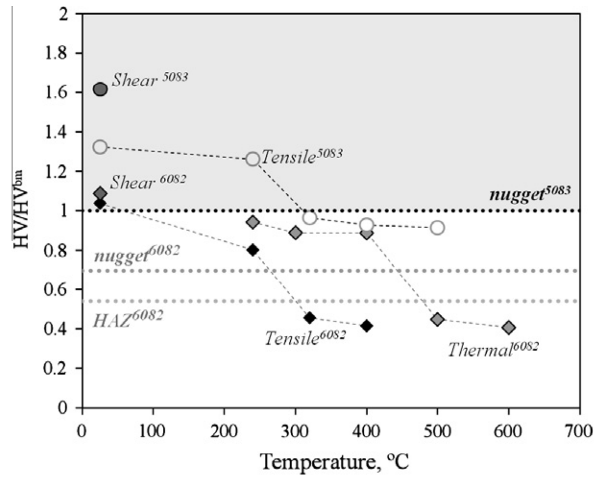

Fig. 8. Hardness ratio (HV/HV^{bm}) versus temperature (HV – average hardness corresponding to the welds and mechanical and thermal simulation samples; HV^{bm} – initial base material hardness).

From Fig. 4, where are plotted the transverse and longitudinal hardness profiles for the AA6082 reference weld, it was already concluded that the overaged HAZ domain encompasses the full perimeter in front of the tool. This material, which displays flow softening at increasing plastic deformation and temperatures, will be easily dragged by the toll into the shear layer surrounding the pin, where the weld is formed [19]. In the shear layer, where the overaged HAZ material will be subjected to intense non-uniform deformation, for one or more tool revolutions, precipitate dissolution will be facilitated by the large number of moving dislocations [33] originating new small coherent particles which will be dispersed in the plastically deformed volume. This will contribute for improving the local strength in the nugget, relative to the surrounding HAZ, as is shown in Figs. 4 and 8 (*nugget*^{6082} results).

Contrary to that registered for the AA6082 weld, for the AA5083 weld no hardness decrease relative to the base material was registered, nor in the TMAZ, nor in the HAZ around the tool, as it was already shown in Fig. 5, where are displayed the transverse and longitudinal hardness profiles for the AA5083 reference weld. Comparing now in Fig. 8 the hardness ratios (HV/HV^{5083}) corresponding to the AA5083 tensile samples (*Tensile*^{5083} results) with the hardness ratio corresponding to the weld (*nugget*^{5083}), it is possible to conclude that, contrarily to the weld, the tensile samples display some hardness decrease relative to the base material. Actually, since this alloy displayed steady flow behaviour during the high temperature tensile tests, which is traditionally attributed to the occurrence of intense recovery during plastic deformation, after tensile testing it is expected that the recovered samples microstructure have lower hardness than the moderately strain-hardened base material, in the H111 condition. It is also important to stress that during welding, despite base material is subjected to high temperature plastic deformation, the strain rates are well above the quasi-static limits [3,10,14,39,40]. At very high strain rates, the dislocation generation rate may rise to a level that reduces the effective time for recovery, resulting in a less recovered structure and increased flow stresses with plastic deformation [31]. This behaviour, which explains the higher hardness values of the weld relative to the tensile samples, also points for increased difficulties in welding the AA5083 alloy. At high strain rates, the increase in flow stress with plastic deformation would prevent intense plastic flow under constant load, which explains the very small amount of material dragged by the toll evidenced by the AA5083 weld cross-sections in Fig. 1. However, it is also important to point that the level of hardening during plastic deformation at high temperatures and strain rates, such as in FSW, is much lower than that experienced during plastic deformation at room temperature or at 240 °C, as it is possible to deduce by comparing in Fig. 8 the hardness ratios for the shear ($Shear^{5083}$) and tensile ($Tensile^{5083}$) samples with that of the weld ($nugget^{5083}$).

Finally, the differences in contact conditions at the tool-workpiece interface, depicted by analysing Fig. 1, can also be explained based in the plastic properties of the base materials. According to Schmidt and Hattel [3], during tool plunge and the first part of the dwell period, a large amount of heat is generated by frictional dissipation, increasing the temperature of the under-shoulder material. Consequently, under similar axial load conditions, the extreme thermal softening experienced by the AA6082 alloy will lead to further submerging of the tool, relatively to the AA5083 alloy, which explains the strong differences in contact area between the AA6082 and AA5083 welds, especially evident for the very low axial load situation illustrated in Fig. 1e and f. Schmidt and Hattel [3] also advocate that sticking conditions at the tool-workpiece interface will be developed when the friction shear stress at the interface exceeds the yield shear stress of the underlying base material. Present results show that sticking conditions will easily develop during FSW of the AA6082 alloy, which presents decreasing flow stress with plastic deformation, and sliding or partial sliding/sticking conditions will prevail for the work-hardenable AA5083 alloy.

5. Conclusions

The influence of the high temperature plastic behaviour of two aluminium alloys, very popular in welding construction, on friction stir weldability, was analysed in this work. It was found that the AA6082 alloy, which according to the base materials mechanical characterisation results, is sensitive to intense flow softening during high temperature plastic deformation, displays good weldability in FSW. For the AA5083 alloy, which according to the base materials mechanical characterisation results, displays steady flow behaviour at increasing temperatures, a very poor weldability was registered under the same welding conditions of the AA6082-T6 alloy. This behaviour results from the strong influence of the plastic properties of the base materials, at high temperatures, on material flow during welding, as well as on contact conditions at the tool workpiece interface. The very important influence of base material plastic properties on friction stir weldability depicted in this work, was never addressed before in FSW literature, which traditionally relates material flow during welding, as well as welds morphology and defects, with tool geometry and/or processing conditions.

Acknowledgements

The authors are indebted to the Portuguese Foundation for the Science and Technology (FCT) and FEDER for the financial support.

References

[1] Nandan R, DebRoy T, Bhadeshia HKDH. Recent advances in friction-stir welding – process, weldment structure and properties. Prog Mater Sci 2008;53:980–1023.
[2] Song M, Kovacevic R. Thermal modeling of friction stir welding in a moving coordinate system and its validation. Int J Mach Tools Manuf 2003;43:605–15.
[3] Schmidt H, Hattel J. A local model for the thermomechanical conditions in friction stir welding. Modell Simul Mater Sci Eng 2005;13:77–93.
[4] Colegrove PA, Shercliff HR, Zettler R. Model for predicting heat generation and temperature in friction stir welding from the material properties. Sci Technol Weld Joining 2007;12:284–97.
[5] Arora A, Nandan R, Reynolds AP, DebRoy T. Torque, power requirement and stir zone geometry in friction stir welding through modeling and experiments. Scripta Mater 2009;60:13–6.
[6] Assidi M, Fourment L, Guerdoux S, Nelson T. Friction model for friction stir welding process simulation: calibrations from welding experiments. Int J Mach Tools Manuf 2010;50:143–55.
[7] Jamshidi Aval H, Serajzadeh S, Kokabi AH. Evolution of microstructures and mechanical properties in similar and dissimilar friction stir welding of AA5086 and AA6061. Mater Sci Eng A 2011;528:8071–83.
[8] Khandkar MZH, Khan JA, Reynolds AP. Prediction of temperature distribution and thermal history during friction stir welding: input torque based model. Sci Technol Weld Joining 2003;8:165–74.
[9] Miles MP, Decker BJ, Nelson TW. Formability and strength of friction-stir-welded aluminum sheets. Metall Mater Trans A 2004;35A:3461–8.
[10] Colegrove PA, Shercliff HR. CFD modelling of friction stir welding of thick plate 7449 aluminium alloy. Sci Technol Weld Joining 2006;11:429–41.
[11] Ren SR, Ma ZY, Chen LQ. Effect of welding parameters on tensile properties and fracture behavior of friction stir welded Al–Mg–Si alloy. Scripta Mater 2007;56:69–72.
[12] Cabibbo M, McQueen HJ, Evangelista E, Spigarelli S, Di Paola M, Falchero A. Microstructure and mechanical property studies of AA6056 friction stir welded plate. Mater Sci Eng A 2007;460–461:86–94.
[13] Hwang Y-M, Kang Z-W, Chiou Y-C, Hsu H-H. Experimental study on temperature distributions within the workpiece during friction stir welding of aluminum alloys. Int J Mach Tools Manuf 2008;48:778–87.
[14] Nandan R, Roy G, Debroy T. Numerical simulation of three-dimensional heat transfer and plastic flow during friction stir welding. Metall Mater Trans A 2006;37:1247–59.
[15] Jacquin D, de Meester B, Simar A, Deloison D, Montheillet F, Desrayaud C. A simple Eulerian thermomechanical modeling of friction stir welding. J Mater Process Technol 2011;211:57–65.
[16] Jayaraman M, Sivasubramanian R, Balasubramanian V. Establishing relationship between the base metal properties and friction stir welding process parameters of cast aluminium alloys. Mater Des 2010;31:4567–76.
[17] Balasubramanian V. Relationship between base metal properties and friction stir welding process parameters. Mater Sci Eng A 2008;480:397–403.
[18] Rodrigues DM, Leitão C, Louro R, Gouveia H, Loureiro A. High speed friction stir welding of aluminium alloys. Sci Technol Weld Joining 2010;14:676–81.
[19] Leal RM, Leitão C, Loureiro A, Rodrigues DM, Vilaça P. Material flow in heterogeneous friction stir welding of thin aluminium sheets: effect of shoulder geometry. Mater Sci Eng A 2008;498:384–91.
[20] Leitão C, Leal RM, Rodrigues DM, Vilaça P, Loureiro A. Material flow in friction stir welding. Microsc Microanal 2008;14:87–90.
[21] Leitão C, Leal RM, Rodrigues DM, Loureiro A, Vilaça P. Mechanical behaviour of similar and dissimilar AA5182-H111 and AA6016-T4 thin friction stir welds. Mater Des 2009;30:101–8.
[22] Rodrigues DM, Loureiro A, Leitão C, Leal RM, Chaparro BM, Vilaça P. Influence of friction stir welding parameters on the microstructural and mechanical properties of AA 6016-T4 thin welds. Mater Des 2009;30:1913–21.
[23] Tronci A, McKenzie R, Leal RM, Rodrigues DM. Microstructural and mechanical characterisation of 5XXX-H111 friction stir welded tailored blanks. Sci Technol Weld Joining 2011;16:433–9.
[24] Leitão C, Galvão I, Leal RM, Rodrigues DM. Determination of local constitutive properties of aluminium friction stir welds using digital image correlation. Mater Des 2012;33:69–74.
[25] ASTM E8M-04. Standard test methods for tension testing of metallic materials (Metric).
[26] ASTM E21-98. Standard test methods for elevated temperature tension tests of metallic materials.
[27] Zhang Z, Chen JT. The simulation of material behaviors in friction stir welding process by using rate-dependent constitutive model. J Mater Sci 2008;43:222–32.
[28] Rosales MJC, Alcantara NG, Santos J, Zettler R. The backing bar role in heat transfer on aluminium alloys friction stir welding. In: Rosa LGMF, editor. Mater Sci Forum; 2010. p. 459–64.
[29] Sato YS, Park SHC, Kokawa H. Microstructural factors governing hardness in friction-stir welds of solid-solution-hardened Al alloys. Metall Mater Trans A 2001;32:3033–42.
[30] Upadhyay P, Reynolds AP. Effects of thermal boundary conditions in friction stir welded AA7050-T7 sheets. Mater Sci Eng A 2010;527:1537–43.
[31] Zhou M, Clode MP. Constitutive equations for modelling flow softening due to dynamic recovery and heat generation during plastic deformation. Mech Mater 1998;27:63–76.
[32] Cerri E, Evangelista E, Ryum N. On the effect of plastic deformation on the coarsening of theta-phase precipitation in an Al–Cu alloy. Metall Mater Trans A 1997;28:257–63.
[33] Verlinden B, Wouters P, McQueen HJ, Aernoudt E, Delaey L, Cauwenberg S. Effect of different homogenization treatments on the hot workability of aluminum alloy – AA2024. Mater Sci Eng A 1990;123:229–37.

[34] Wouters P, Verlinden B, McQueen HJ, Aernoudt E, Delaey L, Cauwenberg S. Effect of homogenization and precipitation treatments on the hot workability of an aluminium alloy AA2024. Mater Sci Eng A 1990;123:239–45.
[35] ASM. ASM Handbook – Fractography; 1987.
[36] Zhang Z, Zhang H. Material behaviors and mechanical features in friction stir welding process. Int J Adv Manuf Technol 2007;35:86–100.
[37] Su JQ, Nelson TW, Mishra R, Mahoney M. Microstructural investigation of friction stir welded 7050-T651 aluminium. Acta Mater 2003;51:713–29.
[38] Amancio-Filho ST, Sheikhi S, dos Santos JF, Bolfarini C. Preliminary study on the microstructure and mechanical properties of dissimilar friction stir welds in aircraft aluminium alloys 2024-T351 and 6056-T4. J Mater Process Technol 2008;206:132–42.
[39] Sato YS, Takauchi H, Park SHC, Kokawa H. Characteristics of the kissing-bond in friction stir welded Al alloy 1050. Mater Sci Eng A 2005;405:333–8.
[40] Nandan R, Roy GG, Lienert TJ, Debroy T. Three-dimensional heat and material flow during friction stir welding of mild steel. Acta Mater 2007;55:883–95.